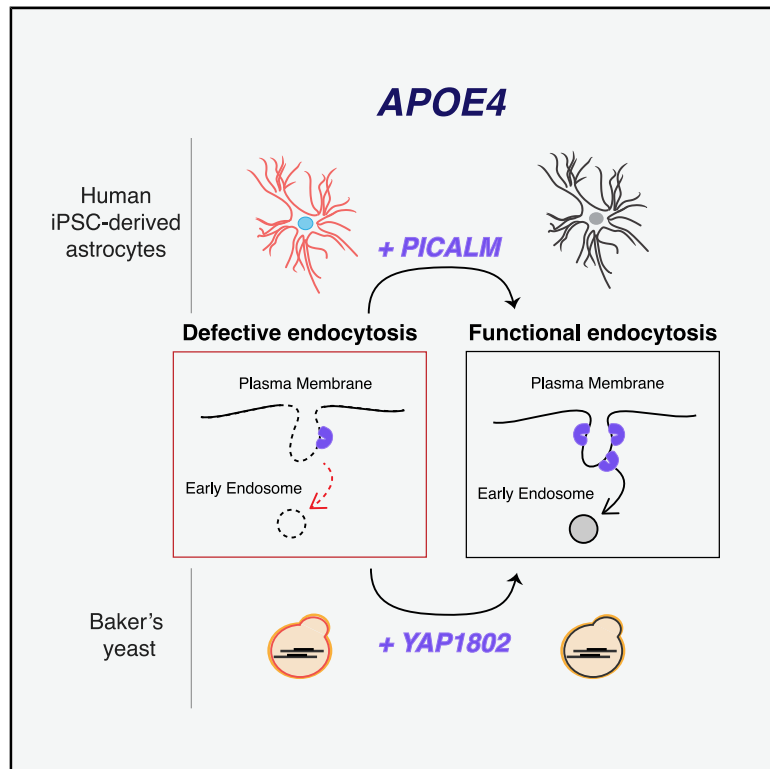# *PICALM* Rescues Endocytic Defects Caused by the Alzheimer's Disease Risk Factor *APOE4*

Graphical Abstract

Authors

Priyanka Narayan, Grzegorz Sienski, Julia M. Bonner, ..., M. Inmaculada Barrasa, Li-Huei Tsai, Susan Lindquist

Correspondence

lhtsai@mit.edu

In Brief

APOE4 is the strongest genetic risk factor for late-onset Alzheimer's disease (AD). Narayan and Sienski et al. find that *APOE4* disrupts early endocytosis, a process by which cells take up external material. By increasing the levels of another AD risk factor, *PICALM*, the authors are able to reverse these disruptions.

Highlights

- *APOE4* disrupts early endocytic trafficking in iPSC-derived astrocytes

- We establish an *APOE4* yeast model in which *APOE4* affects early endocytic trafficking

- *Yap1802*, the yeast homolog of human *PICALM*, suppresses endocytic defects in *APOE4* yeast

- Increasing *PICALM* expression reverses endocytic defects in *APOE4* astrocytes

CellPress

Report

PICALM Rescues Endocytic Defects Caused by the Alzheimer's Disease Risk Factor *APOE4*

Priyanka Narayan,[1,2,6,7] Grzegorz Sienski,[1,7,8] Julia M. Bonner,[1,2] Yuan-Ta Lin,[2] Jinsoo Seo,[2] Valeriya Baru,[1] Aftabul Haque,[1] Blerta Milo,[2] Leyla A. Akay,[2] Agnese Graziosi,[2] Yelena Freyzon,[1] Dirk Landgraf,[1] William R. Hesse,[1] Julie Valastyan,[1] M. Inmaculada Barrasa,[1] Li-Huei Tsai,[2,3,10,*] and Susan Lindquist[1,4,5,9]

[1]Whitehead Institute for Biomedical Research, Cambridge, MA 02142, USA
[2]Picower Institute for Learning and Memory, Massachusetts Institute of Technology, Cambridge, MA 02139, USA
[3]Department of Brain and Cognitive Sciences, Massachusetts Institute of Technology, Cambridge, MA 02139, USA
[4]Department of Biology, Massachusetts Institute of Technology, Cambridge, MA 02139, USA
[5]Howard Hughes Medical Institute, Cambridge, MA 02139, USA
[6]Genetics and Biochemistry Branch, NIDDK, National Institutes of Health, Bethesda, MD 20814, USA
[7]These authors contributed equally
[8]Present address: Discovery Biology, Discovery Sciences, BioPharmaceuticals R&D, AstraZeneca, Gothenburg, Sweden
[9]Deceased
[10]Lead Contact
*Correspondence: lhtsai@mit.edu
https://doi.org/10.1016/j.celrep.2020.108224

SUMMARY

The ε4 allele of apolipoprotein E (*APOE4*) is a genetic risk factor for many diseases, including late-onset Alzheimer's disease (AD). We investigate the cellular consequences of *APOE4* in human iPSC-derived astrocytes, observing an endocytic defect in *APOE4* astrocytes compared with their isogenic *APOE3* counterparts. Given the evolutionarily conserved nature of endocytosis, we built a yeast model to identify genetic modifiers of the endocytic defect associated with *APOE4*. In yeast, only the expression of *APOE4* results in dose-dependent defects in both endocytosis and growth. We discover that increasing expression of the early endocytic adaptor protein Yap1802p, a homolog of the human AD risk factor *PICALM*, rescues the *APOE4*-induced endocytic defect. In iPSC-derived human astrocytes, increasing expression of *PICALM* similarly reverses endocytic disruptions. Our work identifies a functional interaction between two AD genetic risk factors—*APOE4* and *PICALM*—centered on the conserved biological process of endocytosis.

INTRODUCTION

Defective intracellular trafficking is a hallmark of neurodegenerative diseases, including Alzheimer's disease (AD) (Neefjes and van der Kant, 2014; Nixon, 2005). Multiple genes identified in genome-wide association studies for late-onset AD implicate endocytosis as a key risk-related process (Lambert et al., 2009, 2013; Naj et al., 2011). Endocytic defects are evident in preclinical stages of sporadic AD, particularly in *APOE4* carriers (Cataldo et al., 2000). Impaired endocytosis in AD is most commonly associated with dysregulated production or poor clearance of β-amyloid (Aβ) (Koo and Squazzo, 1994; Lah and Levey, 2000; Thinakaran and Koo, 2008; Vassar et al., 1999). However, endocytic defects can appear before significant amyloid deposition (Cataldo et al., 2000), suggesting that endocytic processes represent a critical node and possible target for therapeutic intervention.

The ε4 allele of the *APOE* gene (*APOE4*) encoding apolipoprotein E (APOE) is a major genetic risk factor for late-onset AD (Lambert et al., 2009; Strittmatter et al., 1993). The human *APOE* gene exists in three common alleles that differ from one another at just two amino acid positions (112 and 158). These

alleles are present in the population at the following frequencies: 8.4% (*APOE2*, *Cys112/Cys158*), 77.9% (*APOE3*, *Cys112/Arg168*), and 13.7% (*APOE4*, *Arg112/Arg158*). Individuals carrying one *APOE4* allele are 3–4 times more likely to develop AD than those without (Corder et al., 1993; Liu et al., 2013).

Previous studies on the role of *APOE4* in AD risk implicate both Aβ-dependent and Aβ-independent pathways (Cataldo et al., 2000; Liu et al., 2013; Mahley and Rall, 2000; Yu et al., 2014). APOE4 has been reported to interact with the microtubule-associated protein tau (Shi et al., 2017), a key player in many neurodegenerative diseases like AD and Parkinson's disease (Simón-Sánchez et al., 2009). *APOE4* also increases risk for dementia with Lewy bodies (Tsuang et al., 2013). In addition, *APOE4* impairs recovery from traumatic brain injury (Friedman et al., 1999; Houlden and Greenwood, 2006) and has been implicated in the dysfunction of the blood-brain barrier (Blanchard et al., 2020; Zlokovic, 2013).

Although the strong genetic association between *APOE4* and disease risk has been recognized for more than 20 years, the question of how *APOE4* increases disease risk remains unresolved (Yamazaki et al., 2019). *APOE4*'s profound effect on AD risk and the early appearance of disrupted endocytosis in the
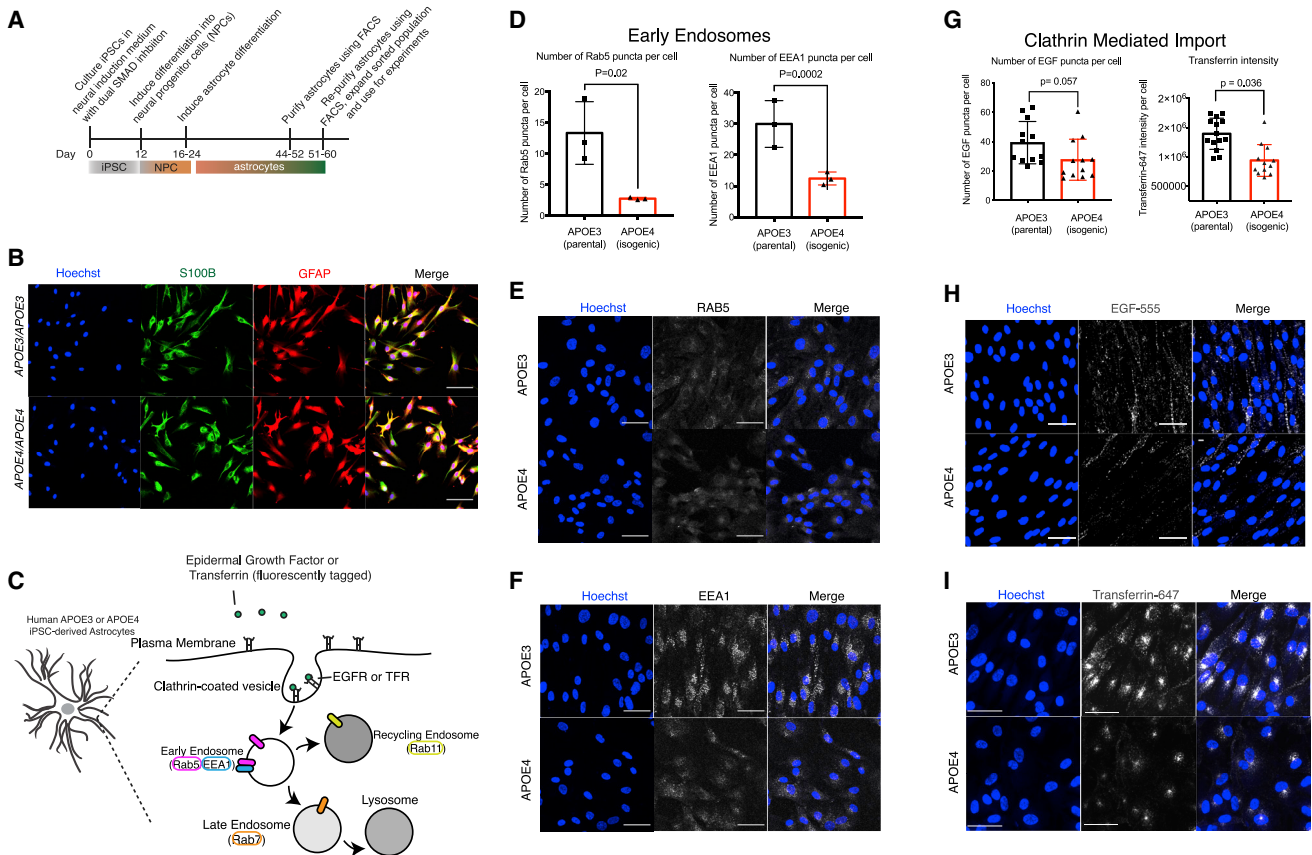
Figure 1. *APOE4*-Expressing iPSC-Derived Astrocytes Exhibit a Defect in Early Endocytosis
(A) Differentiation of iPSCs to astrocytes.
(B) Astrocytes stained for S100β and GFAP. Scale bar, 100 μm.
(C) Schematic of endocytosis steps probed in human *APOE* astrocytes.
(D) Levels of Rab5 (left) and EEA1 (right) staining an isogenic pair of APOE astrocytes. Mean ± SD shown of 80–100 cells per sample for n = 3 samples.
(E and F) Representative images of (E) Rab5 staining and (F) EEA1 staining in *APOE* astrocytes. Scale bar, 50 μm.
(G) Quantification of microscopy images of the number of EGF puncta per cell (left) or the internalization of transferrin per cell (right) in one isogenic pair of APOE astrocytes (*APOE3* parental line). Mean ± SD shown of 30–50 cells per sample for n = 12 samples.
(H and I) Representative images displaying (H) EGF endocytosis and (I) transferrin endocytosis in human *APOE* astrocytes. Scale bar, 50 μm.
See also Figures S1 and S2.

pathogenesis of AD motivated us to (1) characterize the impact of *APOE4* expression on disrupted endocytosis and (2) identify genetic means to reverse these disruptions.

RESULTS

APOE4 Disrupts Endocytosis in iPSC-Derived Astrocytes

Induced pluripotent stem cell (iPSC)-derived cells have been used to recapitulate many molecular aspects of various human diseases (Devine et al., 2011; Park et al., 2008; HD iPSC Consortium, 2012) including AD-relevant consequences of *APOE4* (Lin et al., 2018). We used two independent pairs of cells that are isogenic at all loci except for *APOE*, where they are either *APOE3* or *APOE4*. The pairs were generated using one *APOE3* homozygous parental line and one *APOE4* homozygous parental line (Figure S1A). All iPSC lines used in this study exhibited a

normal karyotype (Figure S1B). Our previous work has shown that *APOE* expression in *APOE4* astrocytes is lower than in isogenic *APOE3* astrocytes (Lin et al., 2018). In addition, we have described abnormal EEA1 staining in iPSC-derived *APOE4* neurons (Lin et al., 2018), suggesting *APOE4* could affect endocytic processes.

We chose to focus our study on iPSC-derived astrocytes (Chen et al., 2014) (Figure 1A), because astrocytes are the predominant source of APOE in the human brain (Liu et al., 2013). We confirmed that our astrocytes were positive for the astrocytic markers S100β and GFAP (Figure 1B) and do not express markers of other potentially contaminating cell types (Figure S1C). We systematically interrogated multiple stages of the endocytic pathway to identify whether *APOE4* astrocytes displayed endocytic perturbations when compared with their isogenic *APOE3* counterparts (Figure 1C). We first examined immunofluorescence staining of Rab proteins and Rab effector

proteins that specifically mark early, late, and recycling endosomes. We visualized the number of early endosomes directly using immunofluorescent probes against the early endosome-associated proteins Rab5 and EEA1. We observed that the number of both Rab5-positive and EEA1-positive puncta were decreased in *APOE4* compared with *APOE3* astrocytes (Figures 1D–1F). We used a similar approach to examine late endosomes (Rab7 positive) and recycling endosomes (Rab11 positive). In contrast to our finding in early endocytic effectors, we noted no difference in Rab11 (recycling endosome) levels between astrocytes of the *APOE3* and *APOE4* genotype (Figures S2A and S2B). *APOE4* astrocytes also exhibited a trend toward lower late endosomal and lysosomal numbers when compared with *APOE3* astrocytes in both isogenic pairs (Figures S2C–S2F). These findings were not a result of differential expression of these endosomal markers between *APOE3* and *APOE4* astrocytes (Figure S2G). In fact, EEA1 levels detected by western blot were considerably lower in *APOE4* astrocytes than in their *APOE3* counterparts (Figure S2H), suggesting that changes in levels of endocytic proteins result from altered recruitment and turnover of these proteins. These results reveal that early endocytosis is the most affected stage of endocytosis when comparing *APOE4* and *APOE3* astrocytes.

To determine whether the differences observed in the accumulation of early endocytic vesicles resulted in functional defects in early endocytosis, we used fluorescently tagged ligands (epidermal growth factor [EGF] and transferrin [Tf]) to examine the early stages of clathrin-mediated internalization (Harding et al., 1983). By exposing cells to a 5-min pulse of fluorescent EGF, we directly visualized the EGF taken up by the early endocytic machinery (Figures 1C, 1G, and 1H). *APOE4* astrocytes trend toward internalizing less EGF (Figures 1G and 1H). Using fluorescently tagged Tf, we again observed that *APOE4* astrocytes internalized less Tf than *APOE3* astrocytes. Altogether, these data suggest that *APOE4* astrocytes display lower rates of early endocytosis than *APOE3* astrocytes (Figures 1G and 1I). Previously generated transcriptomic data on these cells confirmed that the effects were not due to decreased expression of the EGF or Tf receptors in the *APOE4* astrocytes when compared with their *APOE3* counterparts (Figure S2G) (Lin et al., 2018). These results were confirmed in astrocytes derived from an independent iPSC line (Figure S1A) (Lin et al., 2018), in which we again observed that *APOE4* astrocytes exhibit a similar genotype-dependent decrease in early clathrin-mediated endocytosis (Figure S2I), as well as a trend toward decrease in late endosome number (Figure S2C). Altogether, our results show that *APOE4* disrupts early endocytosis in human astrocytes.

To assess whether the perturbations to early endocytosis were due to a toxic gain of function or loss of function, we used an *APOE* knockout line generated from the parental *APOE3* line used in our study. This knockout line resulted from an early stop codon and produced no detectable *APOE* mRNA or protein (Blanchard et al., 2020; Lin et al., 2018). In contrast to our *APOE4* lines, *APOE* knockout-derived astrocytes did not exhibit early endocytic perturbations (Figures S2J–S2M). Therefore, we conclude that the endocytic dysfunction results from a toxic gain of function of the APOE4 isoform.

A Yeast *APOE* Model Displays Endocytic Abnormalities in Processes Disrupted in Human Astrocytes

To explore the consequences of *APOE4* on endocytosis in greater detail, we constructed a model of APOE biology in baker's yeast, taking advantage of the evolutionary conservation of mediators and modulators of endomembrane trafficking within eukaryotes (Boettner et al., 2011; Goode et al., 2015; Kachroo et al., 2015). Our yeast model contained stably integrated constructs at known genomic loci under the control of an estradiol-inducible promoter (Aranda-Díaz et al., 2017; McIsaac et al., 2013) expressing the human *APOE* isoforms (Figures 2A, S3A, and S3B). We engineered the construct to include a secretory pathway signal sequence to ensure the APOE4 protein would experience an environment in yeast that is similar to that which it encounters in human cells. APOE isoforms tagged with GFP within our yeast model display endoplasmic reticulum (ER) localization with some puncta in the case of *APOE4* yeast (Figure S3D). Using semi-native gel electrophoresis, we confirmed that unlike another yeast model expressing the toxic Aβ42 peptide using the same promoter and signal sequence (Treusch et al., 2011), APOE4 does not accumulate in protein aggregates (Figure S3E). This finding suggests that the cellular phenotypes we observed are not responses to aberrant protein aggregation and therefore reflect biology relevant to *APOE4*.

Given our observation in iPSC-derived astrocytes, we asked whether our yeast model showed endocytic defects. Early endosomes were indeed abnormal in our *APOE4* yeast model, which displayed disrupted levels and localization of endogenously tagged Rab5 homologs, YPT5 and VPS21 (Figures 2B and 2C), compared with *APOE3* yeast. Using the trafficking of endogenously tagged Ste3p and Mup1p, which serve as sentinels for early endocytic disruption, we again observed defects associated only with expression of *APOE4* (Figures S3E–S3I). We also observed disruptions to late endosomal levels and localization in *APOE4* yeast (Figure S3J). While we observed a decrease in Rab5 and EEA1 in human iPSC-derived *APOE4* astrocytes (Figures 1D–1F), the levels of the yeast homologs were increased in *APOE4* yeast (Figures 2C and 2D). We have previously shown that human iPSC-derived *APOE4* neurons present increased EEA1 staining (Lin et al., 2018), and others have demonstrated a range of endocytic defects associated with APOE4 (Nuriel et al., 2017), suggesting that cell type can greatly influence APOE4 defects and that our yeast model may reflect aspects of multiple human cell types.

To specifically interrogate early endocytosis, we used a quantitative invertase assay (Burston et al., 2009) to assess endocytic efficiency in *APOE3-* and *APOE4*-expressing yeast. This assay uses a transmembrane chimeric protein reporter (GSS) made of an extracellular sucrose invertase enzyme, the yeast protein Snc1p, and a cytosolic GFP. Accumulation of GSS on the cell surface due to impaired endocytosis leads to increased invertase activity, whereas an exocytosis or recycling defect results in a reduction in GSS at the cell surface and thus lower invertase activity. Endocytic efficiency is assessed via an enzymatic assay with a colorimetric readout (Burston et al., 2009; Dalton et al., 2015; Darsow et al., 2000) (Figure 2D). As a control, the deletion of a key early endocytosis factor, *SLA1*, resulted in increased cell surface GSS and therefore a higher invertase signal (Figure 2E).
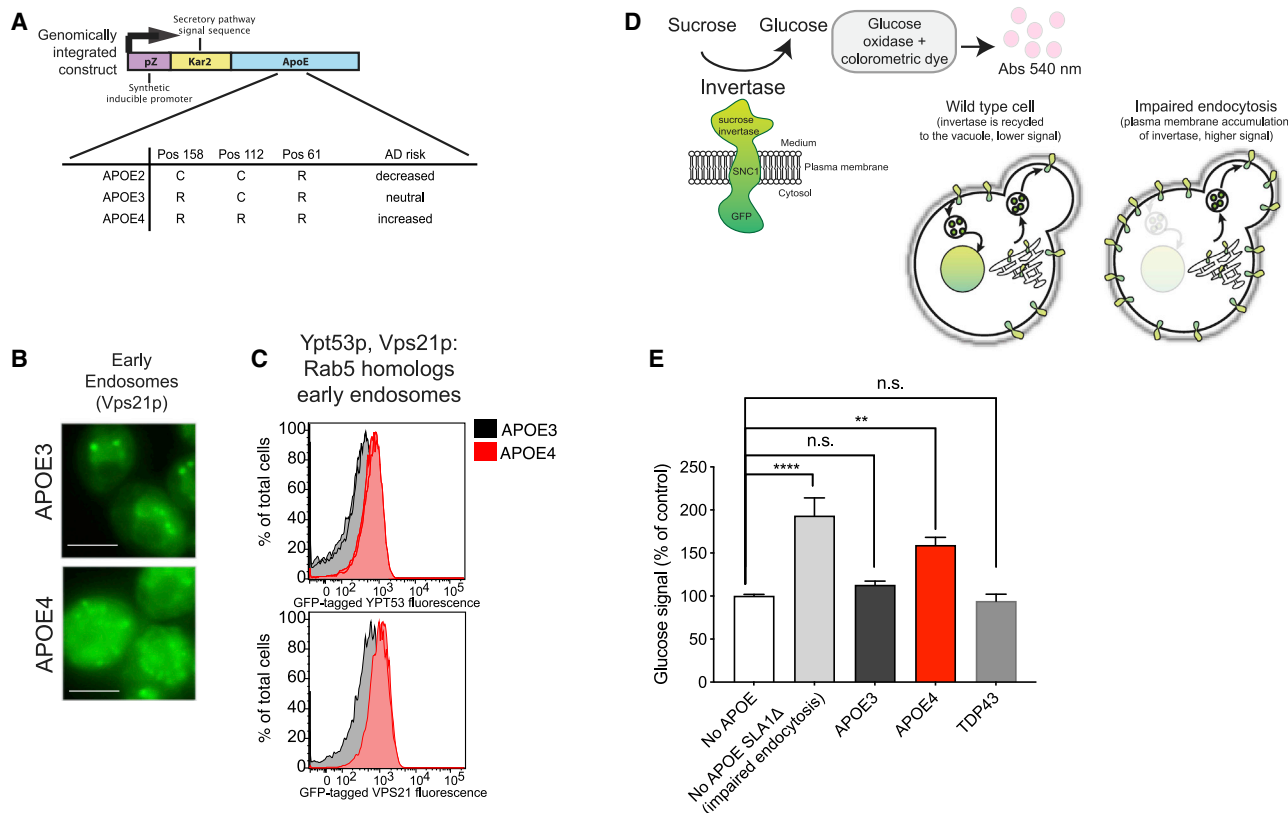
Figure 2. A Yeast Model Faithfully Recapitulates APOE4-Associated Endocytic Defects
(A) Estradiol-inducible promoter system used in the APOE yeast model.
(B) Fluorescence microscopy of the mNeonGreen-tagged Vps21p. Scale bar, 5 μm.
(C) Mean fluorescent signal from mNeonGreen-tagged Vps21p and Ypt53p quantified by flow cytometry, 10,000 cells per sample.
(D) Adapted schematic of the GSS invertase assay.
(E) Glucose signal from invertase assays of the indicated *APOE*-expressing strains and a TDP43-expressing strain. One-way ANOVA followed by Tukey's multiple comparison test (****$p < 0.0001$). Mean ± SD for n = 3 independent colonies.
See also Figure S3.

APOE4-expressing yeast display a clear increase in the invertase signal compared with *APOE3* or wild-type yeast (Figure 2E). Yeast expressing another neurodegenerative disease-associated protein, TDP-43 (Johnson et al., 2008), displayed no significant reduction in invertase activity, suggesting the defect in endocytosis is specific to APOE4.

Our yeast *APOE4* model thus reflects disruption in endocytic processes, particularly in endocytic uptake, similar to those observed in our human iPSC-derived astrocytes and may therefore be used as a tool to identify genetic and chemical factors that could modify this effect of APOE4. However, validation and further analysis of specific mechanisms and pathways must be done in a human cell type-specific manner. We therefore used our yeast model to identify potential genetic modifiers of the early endocytosis disruption in *APOE4*, which we could then investigate in our human iPSC astrocyte system.

YAP1802, the Yeast Homolog of PICALM, Reverses APOE4-Induced Endocytic Disruptions
In our yeast model, a growth defect accompanied *APOE4*-induced perturbations to endocytosis (Figures 3A, 3B, S4A,

and S4B). Despite being expressed at similar levels, *APOE3* did not cause a growth defect (Figures 3A, 3B, S3A, S3B, S4A, and S4B).

We performed a screen for suppressors of the APOE4-induced growth defect and then examined their effects on our endocytic phenotypes. First, we profiled a set of 34 proteins involved in all stages of endocytic trafficking (Table S1) (Lu et al., 2016). When overexpressed, only Yap1802p significantly affected the *APOE4* yeast growth phenotype (Figure 3C, highlighted in yellow). Yap1802p is an early endocytic adaptor protein that participates in the budding of early endocytic vesicles. We also observed that two other early endocytic proteins, Ede1p and Aps2p, displayed non-significant trends toward modification of the *APOE4* yeast growth phenotype. Together, these data suggest that disruptions to the endocytic pathway observed in our yeast and iPSC models arise at least partly from defects in early endocytosis and that, in yeast, this is sufficient to modulate growth.

We asked whether increasing expression of *YAP1802* altered levels of APOE4 by immunoblotting or fluorescence of a GFP-tagged APOE construct (Figures S4D and S4E). Because
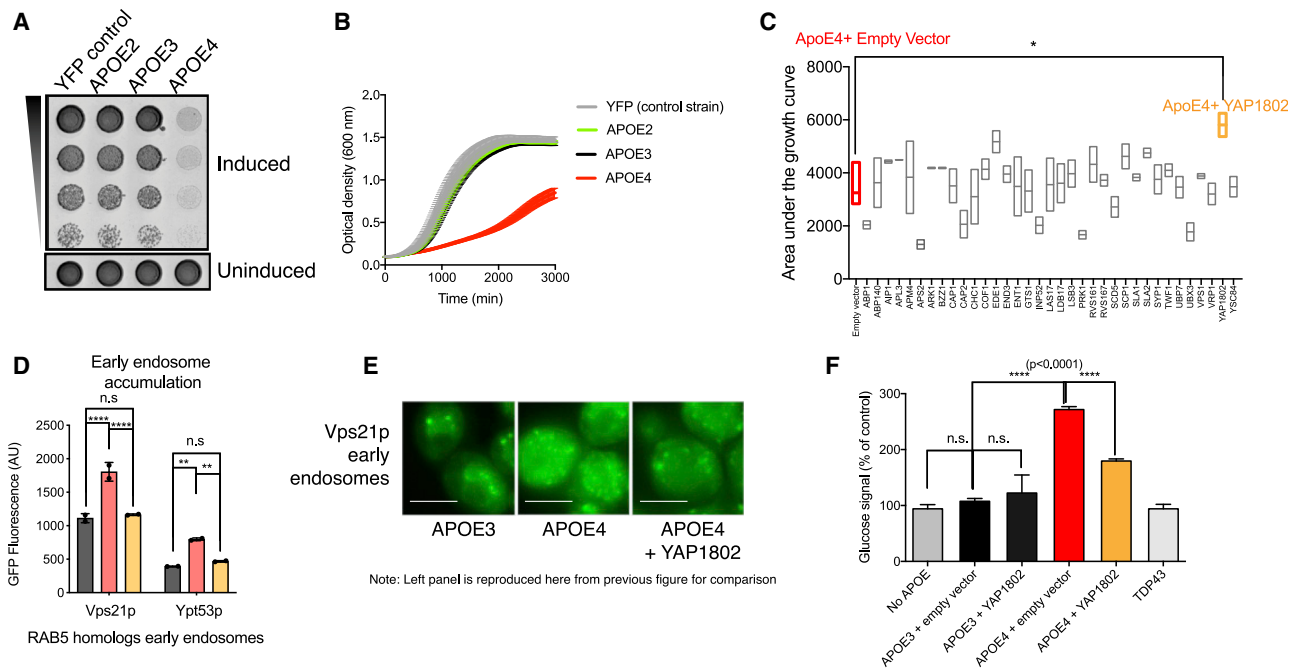
Figure 3. APOE4-Associated Endocytic Defects in Yeast Can Be Rescued by Increased Expression of *YAP1802*

(A and B) Growth of *APOE* yeast strains on (A) solid inducing (75 nM estradiol) or non-inducing media (no estradiol) and (B) liquid inducing (7.5 nM estradiol) or uninduced (no estradiol) media. Error bars are SD of n = 4 trials.

(C) Area under the growth curves for overexpressed endocytosis-related proteins on an *APOE4* background. Ordinary one-way ANOVA followed by Dunnett's multiple comparison test (*p < 0.05), n = 4 transformants per modifier, min to max with line at median.

(D) Mean fluorescent signal of mNeonGreen-tagged Rab5 homologs, quantified by flow cytometry. 10,000 cells per sample, 2 samples per condition shown. Two-way ANOVA followed by Tukey's multiple comparison test (****p < 0.0001, **p < 0.01).

(E) Fluorescence microscopy of mNeonGreen-tagged Vps21p. Scale bar, 5 μm.

(F) Glucose signal from invertase assays of the indicated *APOE*-expressing strains with and without co-expression of *YAP1802* and a TDP43-expressing strain. One-way ANOVA followed by Tukey's multiple comparison test (****p < 0.0001). Mean ± SD for n = 3 independent colonies.

See also Figure S4 and Table S1.

we did not observe a change in APOE4 levels in these assays, we concluded that increasing *YAP1802* expression can uncouple the presence of APOE4 from its detrimental effects.

We examined whether overexpression of Yap1802p could modify the dysregulation observed in Rab proteins. Increasing expression of Yap1802p restored the accumulated levels of Rab5 homologs observed in the *APOE4*-expressing strains to lower, *APOE3*-like levels (Figure 3D). Increasing Yap1802p expression also restored the localization of Vps21p, a Rab5 homolog, to a less diffuse, *APOE3*-like pattern (Figure 3E).

Finally, we asked whether the growth defect rescue by Yap1802p was accompanied by a rescue of the APOE4-induced defect in early endocytosis. Indeed, overexpression of Yap1802p resulted in significant reduction of the GSS invertase signal, indicating that Yap1802p expression can functionally rescue APOE4-induced trafficking defects (Figure 3F).

PICALM Overexpression Rescues an *APOE4*-Induced Disruption of Endocytosis in iPSC-Derived Astrocytes

Our *APOE4* yeast model suggested that *YAP1802* is a robust genetic modifier of the *APOE4*-induced endocytic defect. The human homolog of *YAP1802* is *PICALM*, which is itself implicated

in AD. We therefore examined whether *PICALM* could modify *APOE4* phenotypes in iPSC-derived human astrocytes.

Having confirmed that endogenous expression of *PICALM* was not significantly different between *APOE3* and *APOE4* astrocytes (Figure S4F), we treated *APOE3* and *APOE4* astrocytes with a lentivirus driving the expression of *PICALM* expressed with a hemagglutinin (HA) tag (PICALM-HA) under an astrocyte-specific *GFAP* promoter (Figures 4A and 4B). Because modifying endocytosis may enhance or reduce rates of internalization, recycling, or degradation of proteins (Antonescu et al., 2014), we confirmed that expression of *PICALM* did not change APOE levels (Figures 4C and 4D).

To examine the effect of *PICALM* overexpression on *APOE4*-induced endocytic disruptions, we again used the fluorescent ligands, EGF and Tf, as probes of the early endocytic process. We found that overexpression of *PICALM* increased EGF uptake (Figures 4A, 4E, and 4F) and Tf uptake (Figures 4G and 4H), suggesting restoration of early endocytic capacity. Although not significant, we observed a trend toward increased EEA1-positive puncta volume and intensity in *APOE4* astrocytes with increased expression of *PICALM* (Figures S4H and S4I). We observed that *PICALM* overexpression induced an endocytic defect in *APOE3*
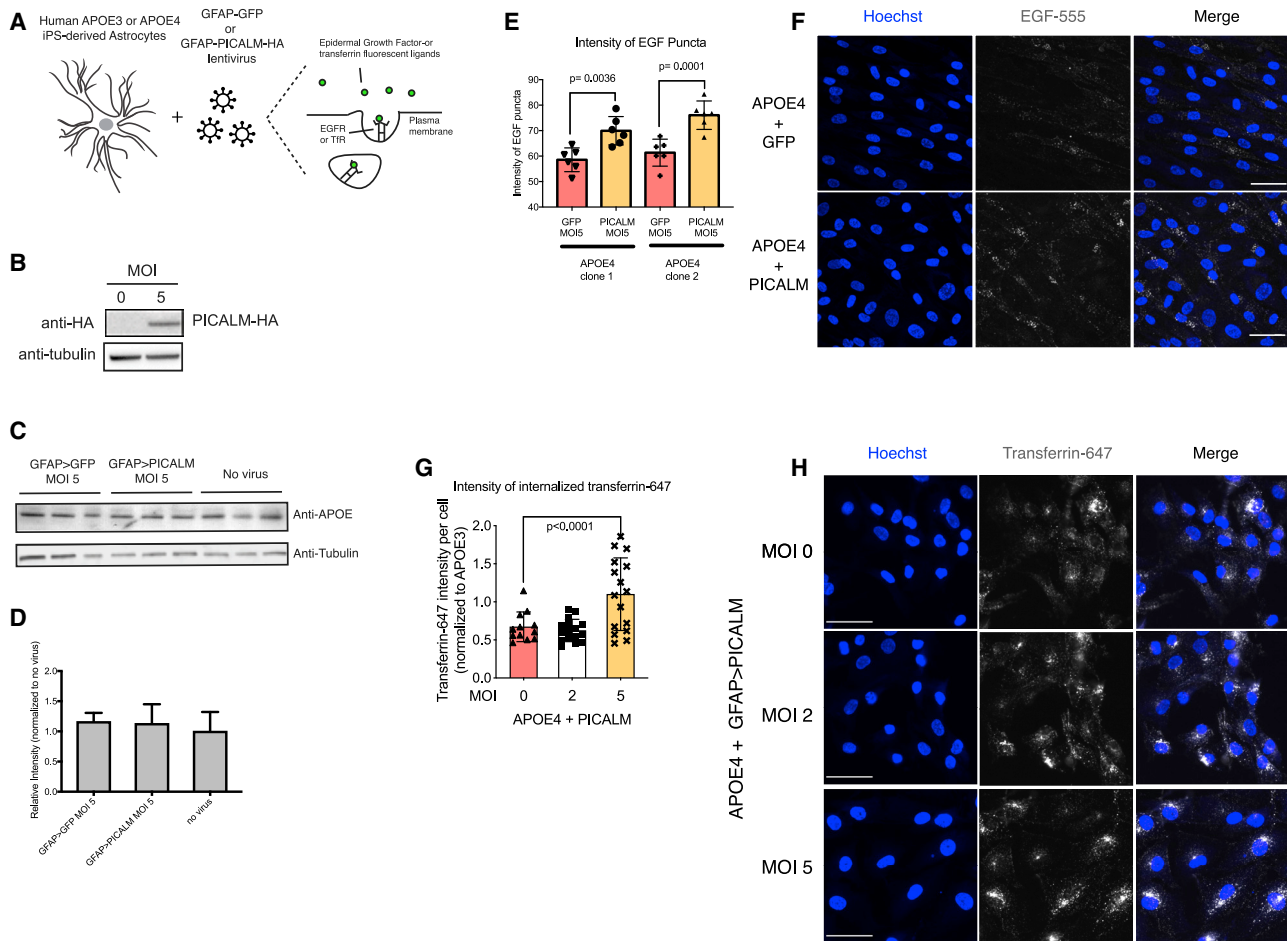
Figure 4. Increasing PICALM Expression Rescues APOE4-Induced Endocytic Defect in iPSC-Derived Astrocytes
(A) Schematic assays fluorescent epidermal growth factor (EGF) or transferrin (Tf).
(B) Western blot of PICALM-HA in iPSC-derived human astrocytes after transduction with a lentivirus expressing PICALM tagged with an HA tag.
(C and D) Western blot (C) and quantification (D) of APOE levels in primary human astrocytes treated with PICALM and GFP viruses (MOI 5). Mean ± SD of n = 3. Student's t test (**p < 0.01, ***p < 0.001), n = 3 experiments.
(E and F) Quantification (E) of the intensity of EGF puncta per cell and representative images (F). Mean ± SD of 80–100 cells per sample. Scale bar, 50 μm.
(G and H) Quantification (G) of Tf internalization and representative images (H) with and without GFAP-PICALM-HA virus. Tukey's multiple comparison test. Mean ± SD of 80–100 cells per sample. Scale bar, 50 μm.
See also Figure S4.

astrocytes (Figure S4G). This concurs with previous work that noted overexpression of *PICALM* in a normal context may impair endocytosis (Tebar et al., 1999). These results suggest that the *PICALM*-mediated rescue observed for *APOE4* is allele specific. Altogether, these results demonstrate that increasing the cellular dose of *PICALM* uncouples the presence of *APOE4* from its detrimental effects on endocytosis.

DISCUSSION

In this study, we apply genetic and functional analysis in iPSC-derived astrocytes and yeast to characterize a conserved perturbation to endocytosis associated with APOE4. Through these studies, we identify *PICALM* as a modifier of *APOE4*-associated defects. These findings align well with previous work showing that SNPs that lower expression of *PICALM* are associated with AD risk, whereas SNPs that increase *PICALM* expression decrease AD risk (Morgen et al., 2014; Parikh et al., 2014; Zhao et al., 2015).

Genetic links between *APOE4* and *PICALM* have been previously described (Harold et al., 2009; Lambert et al., 2009; Morgen et al., 2014). However, no clear functional connection has been reported between these risk factors. Given the shared action of these two risk factors on endocytosis, targeting of this cellular pathway could serve as a potential therapeutic avenue.

Prior studies examining APOE4's role in trafficking have largely focused on the trafficking of specific AD-associated proteins like APP and its cleavage product, Aβ. In this study, we

show that APOE4 can disrupt endocytosis independent of APP or Aβ. This finding suggests that disruptions to endocytosis could be a common defect among the many diseases for which APOE4 increases risk.

In neuronal and glial cell types in which endocytic trafficking is critical to cellular function, even a mild disruption to endocytosis may profoundly change intracellular dynamics of many substrates. Chronic perturbation of trafficking pathways over the lifetime of an individual could lead to a disease-vulnerable cellular environment, which could be exacerbated by other environmental or other genetic factors. Broad endocytic disruption may manifest as different phenotypic consequences in different cell types or brain regions, which may then lead to disease-specific consequences of *APOE4*.

This study examined the cellular consequences of the *APOE4* allele in comparison to the *APOE3* allele, considered the neutral allele with respect to AD risk. The *APOE2* allele, which is considered protective with respect to AD risk, may act on similar or different pathways. We anticipate that future studies of *APOE2*, especially in the context of early endocytic disruptions, will expand our understanding of risk for or resilience to AD.

Our work has set up a paradigm to explore genotype-to-phenotype relationships. With advances in high-throughput sequencing, this type of investigation can be extended to understand particular combinations of polymorphisms present in various patient populations. Our study identified the interplay between two AD risk factors, *APOE4* and *PICALM*. The techniques and systems used in this study can be used to systematically interrogate combinations of risk factors or protective factors to understand their impacts on cell biology. Given the genetic heterogeneity of AD and other late-onset neurodegenerative diseases, such studies will offer opportunities for genetic stratification, as well as the identification of targeted therapies for complex diseases.

STAR★METHODS

Detailed methods are provided in the online version of this paper and include the following:

- KEY RESOURCES TABLE
- RESOURCE AVAILABILITY
  - Lead Contact
  - Materials Availability
  - Data and Code availability
- EXPERIMENTAL MODEL AND SUBJECT DETAILS
  - Inducible expression of *APOE* isoforms in *S. cerevisiae*
  - Yeast growth curves in liquid media and spotting assays
  - Semi-denaturing oligomer blots
  - Western blots
  - Reporter assays
  - Invertase assay
  - iPSC culture, derivation, and lentiviral production
  - Immunostaining
  - Transferrin uptake, EGF uptake, and Lysotracker staining
- QUANTIFICATION AND STATISTICAL ANALYSIS

AUTHOR CONTRIBUTIONS

DECLARATION OF INTERESTS

REFERENCES

Antonescu, C.N., McGraw, T.E., and Klip, A. (2014). Reciprocal regulation of endocytosis and metabolism. Cold Spring Harb. Perspect. Biol. *6*, a016964.

Aranda-Díaz, A., Mace, K., Zuleta, I., Harrigan, P., and El-Samad, H. (2017). Robust Synthetic Circuits for Two-Dimensional Control of Gene Expression in Yeast. ACS Synth. Biol. *6*, 545–554.

Blanchard, J.W., Bula, M., Davila-Velderrain, J., Akay, L.A., Zhu, L., Frank, A., Victor, M.B., Bonner, J.M., Mathys, H., Lin, Y.-T., et al. (2020). Reconstruction of the human blood-brain barrier *in vitro* reveals a pathogenic mechanism of APOE4 in pericytes. Nat. Med. *26*, 952–963.

Boettner, D.R., Chi, R.J., and Lemmon, S.K. (2011). Lessons from yeast for clathrin-mediated endocytosis. Nat. Cell Biol. *14*, 2–10.

Burston, H.E., Maldonado-Báez, L., Davey, M., Montpetit, B., Schluter, C., Wendland, B., and Conibear, E. (2009). Regulators of yeast endocytosis identified by systematic quantitative analysis. J. Cell Biol. *185*, 1097–1110.

Cataldo, A.M., Peterhoff, C.M., Troncoso, J.C., Gomez-Isla, T., Hyman, B.T., and Nixon, R.A. (2000). Endocytic pathway abnormalities precede amyloid β deposition in sporadic Alzheimer's disease and Down syndrome: differential effects of APOE genotype and presenilin mutations. Am. J. Pathol. *157*, 277–286.

Chen, C., Jiang, P., Xue, H., Peterson, S.E., Tran, H.T., McCann, A.E., Parast, M.M., Li, S., Pleasure, D.E., Laurent, L.C., et al. (2014). Role of astroglia in Down's syndrome revealed by patient-derived human-induced pluripotent stem cells. Nat. Commun. *5*, 4430.

Corder, E.H., Saunders, A.M., Strittmatter, W.J., Schmechel, D.E., Gaskell, P.C., Small, G.W., Roses, A.D., Haines, J.L., and Pericak-Vance, M.A. (1993). Gene dose of apolipoprotein E type 4 allele and the risk of Alzheimer's disease in late onset families. Science *261*, 921–923.

Dalton, L., Davey, M., and Conibear, E. (2015). Large-scale analysis of membrane transport in yeast using invertase reporters. Methods Mol. Biol. *1270*, 395–409.

Darsow, T., Odorizzi, G., and Emr, S.D. (2000). Invertase fusion proteins for analysis of protein trafficking in yeast. Methods Enzymol. *327*, 95–106.

Devine, M.J., Ryten, M., Vodicka, P., Thomson, A.J., Burdon, T., Houlden, H., Cavaleri, F., Nagano, M., Drummond, N.J., Taanman, J.-W., et al. (2011). Parkinson's disease induced pluripotent stem cells with triplication of the α-synuclein locus. Nat. Commun. *2*, 440.

Friedman, G., Froom, P., Sazbon, L., Grinblatt, I., Shochina, M., Tsenter, J., Babaey, S., Yehuda, B., and Groswasser, Z. (1999). Apolipoprotein E-epsilon4 genotype predicts a poor outcome in survivors of traumatic brain injury. Neurology *52*, 244–248.

Gietz, R.D., and Schiestl, R.H. (2007). High-efficiency yeast transformation using the LiAc/SS carrier DNA/PEG method. Nat. Protoc. *2*, 31–34.

Goode, B.L., Eskin, J.A., and Wendland, B. (2015). Actin and endocytosis in budding yeast. Genetics *199*, 315–358.

Harding, C., Heuser, J., and Stahl, P. (1983). Receptor-mediated endocytosis of transferrin and recycling of the transferrin receptor in rat reticulocytes. J. Cell Biol. *97*, 329–339.

Harold, D., Abraham, R., Hollingworth, P., Sims, R., Gerrish, A., Hamshere, M.L., Pahwa, J.S., Moskvina, V., Dowzell, K., Williams, A., et al. (2009). Genome-wide association study identifies variants at CLU and PICALM associated with Alzheimer's disease. Nat. Genet. *41*, 1088–1093.

HD iPSC Consortium (2012). Induced Pluripotent Stem Cells from Patients with Huntington's Disease Show CAG-Repeat-Expansion-Associated Phenotypes. Cell Stem Cell *11*, 264–278.

Houlden, H., and Greenwood, R. (2006). Apolipoprotein E4 and traumatic brain injury. J. Neurol. Neurosurg. Psychiatry *77*, 1106–1107.

Johnson, B.S., McCaffery, J.M., Lindquist, S., and Gitler, A.D. (2008). A yeast TDP-43 proteinopathy model: Exploring the molecular determinants of TDP-43 aggregation and cellular toxicity. Proc. Natl. Acad. Sci. USA *105*, 6439–6444.

Kachroo, A.H., Laurent, J.M., Yellman, C.M., Meyer, A.G., Wilke, C.O., and Marcotte, E.M. (2015). Evolution. Systematic humanization of yeast genes reveals conserved functions and genetic modularity. Science *348*, 921–925.

Kayatekin, C., Amasino, A., Gaglia, G., Flannick, J., Bonner, J.M., Fanning, S., Narayan, P., Barrasa, M.I., Pincus, D., Landgraf, D., Nelson, J., Hesse, W.R., Costanzo, M., Myers, C.L., Boone, C., Florez, J.C., and Lindquist, S. (2018). Translocon Declogger Ste24 Protects against IAPP Oligomer-Induced Proteotoxicity. Cell *173*, 62–73.e9.

Koo, E.H., and Squazzo, S.L. (1994). Evidence that production and release of amyloid beta-protein involves the endocytic pathway. J. Biol. Chem. *269*, 17386–17389.

Lah, J.J., and Levey, A.I. (2000). Endogenous presenilin-1 targets to endocytic rather than biosynthetic compartments. Mol. Cell. Neurosci. *16*, 111–126.

Lambert, J.-C., Heath, S., Even, G., Campion, D., Sleegers, K., Hiltunen, M., Combarros, O., Zenika, D., Bullido, M.J., Tavernier, B., et al.; European Alzheimer's Disease Initiative Investigators (2009). Genome-wide association study identifies variants at CLU and CR1 associated with Alzheimer's disease. Nat. Genet. *41*, 1094–1099.

Lambert, J.C., Ibrahim-Verbaas, C.A., Harold, D., Naj, A.C., Sims, R., Bellenguez, C., DeStafano, A.L., Bis, J.C., Beecham, G.W., Grenier-Boley, B., et al.; European Alzheimer's Disease Initiative (EADI); Genetic and Environmental Risk in Alzheimer's Disease; Alzheimer's Disease Genetic Consortium; Cohorts for Heart and Aging Research in Genomic Epidemiology (2013). Meta-analysis of 74,046 individuals identifies 11 new susceptibility loci for Alzheimer's disease. Nat. Genet. *45*, 1452–1458.

Lin, Y.-T.J., Gao, F., Feldman, H.M., Wen, H.-L., Penney, J., Cam, H.P., Gjoneska, E., Raja, W.K., Cheng, J., et al. (2018). APOE4 Causes Widespread Molecular and Cellular Alterations Associated with Alzheimer's Disease Phenotypes in Human iPSC-Derived Brain Cell Types. Neuron *98*, 1141–1154.e7.

Liu, C.-C., Liu, C.C., Kanekiyo, T., Xu, H., and Bu, G. (2013). Apolipoprotein E and Alzheimer disease: risk, mechanisms and therapy. Nat. Rev. Neurol. *9*, 106–118.

Lu, R., Drubin, D.G., and Sun, Y. (2016). Clathrin-mediated endocytosis in budding yeast at a glance. J. Cell Sci. *129*, 1531–1536.

Mahley, R.W., and Rall, S.C., Jr. (2000). Apolipoprotein E: far more than a lipid transport protein. Annu. Rev. Genomics Hum. Genet. *1*, 507–537.

McIsaac, R.S., Oakes, B.L., Wang, X., Dummit, K.A., Botstein, D., and Noyes, M.B. (2013). Synthetic gene expression perturbation systems with rapid, tunable, single-gene specificity in yeast. Nucleic Acids Res. *41*, e57.

Morgen, K., Ramirez, A., Frölich, L., Tost, H., Plichta, M.M., Kölsch, H., Rakebrandt, F., Rienhoff, O., Jessen, F., Peters, O., et al. (2014). Genetic interaction of PICALM and APOE is associated with brain atrophy and cognitive impairment in Alzheimer's disease. Alzheimers Dement. *10* (*5 Suppl*), S269–S276.

Naj, A.C., Jun, G., Beecham, G.W., Wang, L.-S., Vardarajan, B.N., Buros, J., Gallins, P.J., Buxbaum, J.D., Jarvik, G.P., Crane, P.K., et al. (2011). Common variants at MS4A4/MS4A6E, CD2AP, CD33 and EPHA1 are associated with late-onset Alzheimer's disease. Nat. Genet. *43*, 436–441.

Neefjes, J., and van der Kant, R. (2014). Stuck in traffic: an emerging theme in diseases of the nervous system. Trends Neurosci. *37*, 66–76.

Nixon, R.A. (2005). Endosome function and dysfunction in Alzheimer's disease and other neurodegenerative diseases. Neurobiol. Aging *26*, 373–382.

Nuriel, T., Peng, K.Y., Ashok, A., Dillman, A.A., Figueroa, H.Y., Apuzzo, J., Ambat, J., Levy, E., Cookson, M.R., Mathews, P.M., and Duff, K.E. (2017). The Endosomal-Lysosomal Pathway Is Dysregulated by *APOE4* Expression *in vivo*. Front. Neurosci. *11*, 702.

Parikh, I., Fardo, D.W., and Estus, S. (2014). Genetics of PICALM expression and Alzheimer's disease. PLoS ONE *9*, e91242.

Park, I.-H., Arora, N., Huo, H., Maherali, N., Ahfeldt, T., Shimamura, A., Lensch, M.W., Cowan, C., Hochedlinger, K., and Daley, G.Q. (2008). Disease-specific induced pluripotent stem cells. Cell *134*, 877–886.

Schneider, C.A., Rasband, W.S., and Eliceiri, K.W. (2012). NIH Image to ImageJ: 25 years of image analysis. Nat Meth *9*, 671–675.

Shi, Y., Yamada, K., Liddelow, S.A., Smith, S.T., Zhao, L., Luo, W., Tsai, R.M., Spina, S., Grinberg, L.T., Rojas, J.C., et al.; Alzheimer's Disease Neuroimaging Initiative (2017). ApoE4 markedly exacerbates tau-mediated neurodegeneration in a mouse model of tauopathy. Nature *549*, 523–527.

Simón-Sánchez, J., Schulte, C., Bras, J.M., Sharma, M., Gibbs, J.R., Berg, D., Paisan-Ruiz, C., Lichtner, P., Scholz, S.W., Hernandez, D.G., et al. (2009). Genome-wide association study reveals genetic risk underlying Parkinson's disease. Nat. Genet. *41*, 1308–1312.

Strittmatter, W.J., Saunders, A.M., Schmechel, D., Pericak-Vance, M., Enghild, J., Salvesen, G.S., and Roses, A.D. (1993). Apolipoprotein E: high-avidity binding to beta-amyloid and increased frequency of type 4 allele in late-onset familial Alzheimer disease. Proc. Natl. Acad. Sci. USA *90*, 1977–1981.

Tebar, F., Bohlander, S.K., and Sorkin, A. (1999). Clathrin assembly lymphoid myeloid leukemia (CALM) protein: localization in endocytic-coated pits,

interactions with clathrin, and the impact of overexpression on clathrin-mediated traffic. Mol. Biol. Cell 10, 2687–2702.

Thinakaran, G., and Koo, E.H. (2008). Amyloid precursor protein trafficking, processing, and function. J. Biol. Chem. 283, 29615–29619.

Treusch, S., Hamamichi, S., Goodman, J.L., Matlack, K.E.S., Chung, C.Y., Baru, V., Shulman, J.M., Parrado, A., Bevis, B.J., Valastyan, J.S., Han, H., Lindhagen-Persson, M., Reiman, E.M., Evans, D.A., Bennett, D.A., Olofsson, A., DeJager, P.L., Tanzi, R.E., Caldwell, K.A., Caldwell, G.A., and Lindquist, S. (2011). Functional links between Aβ toxicity, endocytic trafficking, and Alzheimer's disease risk factors in yeast. Science 334, 1241–1245.

Tsuang, D., Leverenz, J.B., Lopez, O.L., Hamilton, R.L., Bennett, D.A., Schneider, J.A., Buchman, A.S., Larson, E.B., Crane, P.K., Kaye, J.A., et al. (2013). APOE ε4 increases risk for dementia in pure synucleinopathies. JAMA Neurol. 70, 223–228.

Vassar, R., Bennett, B.D., Babu-Khan, S., Kahn, S., Mendiaz, E.A., Denis, P., Teplow, D.B., Ross, S., Amarante, P., Loeloff, R., et al. (1999). β-secretase cleavage of Alzheimer's amyloid precursor protein by the transmembrane aspartic protease BACE. Science 286, 735–741.

Yamazaki, Y., Zhao, N., Caulfield, T.R., Liu, C.-C., and Bu, G. (2019). Apolipoprotein E and Alzheimer disease: pathobiology and targeting strategies. Nat. Rev. Neurol. 15, 501–518.

Yu, J.-T., Tan, L., and Hardy, J. (2014). Apolipoprotein E in Alzheimer's disease: an update. Annu. Rev. Neurosci. 37, 79–100.

Zhao, Z., Sagare, A.P., Ma, Q., Halliday, M.R., Kong, P., Kisler, K., Winkler, E.A., Ramanathan, A., Kanekiyo, T., Bu, G., et al. (2015). Central role for PICALM in amyloid-β blood-brain barrier transcytosis and clearance. Nat. Neurosci. 18, 978–987.

Zlokovic, B.V. (2013). Cerebrovascular effects of apolipoprotein E: implications for Alzheimer disease. JAMA Neurol. 70, 440–444.

STAR★METHODS

KEY RESOURCES TABLE

REAGENT or RESOURCE	SOURCE	IDENTIFIER
Antibodies		
Mouse monoclonal anti-S100B	Atlas Antibodies	AMAB91038 Cat#: AMAb91038, RRID:AB_2665776
Goat polyclonal anti-GFAP	Abcam	ab53554 Cat# ab53554, RRID:AB_880202
Mouse monoclonal anti-Rab5	CST	46449 Cat# 46449, RRID:AB_2799303
Mouse monoclonal anti-EEA1	BD Transduction Laboratories	610457 Cat# 610457, RRID:AB_397830
Rabbit monoclonal anti-Rab7	CST	9367 Cat# 9367, RRID:AB_1904103
Rabbit monoclonal anti-Rab11	CST	5589 Cat# 5589, RRID:AB_10693925
Goat polyclonal anti-APOE	Millipore Sigma	AB947 Cat# AB947, RRID:AB_2258475
Rabbit polyclonal anti-PGK1	Antibodies-online.com	ABIN568371
Rat monoclonal anti-HA (conjugated to HRP)	Roche	12 013 819 001 Cat# 12013819001, RRID:AB_390917
Bacterial and Virus Strains		
pLVX-GFAP-PICALM-HA, *PICALM* overexpression lentivirus	This study	N/A
Chemicals, Peptides, and Recombinant Proteins		
Transferrin-647	Invitrogen	T23366
EGF-555	Invitrogen	E35350
Lysotracker Red	Invitrogen	L7528
B-Estradiol	Sigma Aldrich	E8875-5G
Propidium iodide	Sigma Aldrich	P4864
CSM lacking uracil	Sunrise Science Products	1004-100
CSM lacking uracil and histidine	Sunrise Science Products	1009-100
Experimental Models: Cell Lines		
APOE3/APOE3 parental human iPSC line	Coriell	AG09173
APOE4/APOE4 isogenic human iPSC line	Lin et al., 2018	Lin et al., 2018
APOE4/APOE4 parental human iPSC line	Coriell	AG10788
APOE3/APOE3 isogenic human iPSC line	Lin et al., 2018	Lin et al., 2018
Experimental Models: Organisms/Strains		
S. cerevisiae: Strain background: W303	ATCC	201238
Recombinant DNA		
Invertase GSS reporter construct	Conibear lab	Burston et al., 2009
pNH603-ApoE3	This study	N/A
pNH603-ApoE4	This study	N/A
pNH604-ZEM (pJMB102)	Kayatekin et al., 2018	Kayatekin et al., 2018
pBY011-YAP1802 (FLEXGene library clone)	DNASU.org	ScCD00094178
Software and Algorithms		
GraphPad Prism	GraphPad Software	https://www.graphpad.com/scientific-software/prism/
Imaris	Oxford Instruments	https://imaris.oxinst.com/
ImageJ	Schneider et al., 2012	https://imagej.net/Welcome
FlowJo v8	FlowJo	https://www.flowjo.com/solutions/flowjo/downloads

RESOURCE AVAILABILITY

Lead Contact

Further information and requests for resources and reagents should be directed to and will be fulfilled by the Lead Contact, Li-Huei Tsai (tsaiasst@mit.edu).

Materials Availability

All unique reagents generated in this study are available from the Lead Contact and may require completion of a Materials Transfer Agreement.

Data and Code availability

No custom code was used in this study.

EXPERIMENTAL MODEL AND SUBJECT DETAILS

iPSC-derived lines were generated from the parent lines Coriell #AG09173 and #AG10788 (both female). Line maintenance and derivation into various cell types was performed as previously described (Lin et al., 2018). After sorting, astrocytes derived from these iPSCs were maintained in 100 mm dishes or T75 flasks at 37°C, 5% CO_2 in Astrocyte Medium (ScienCell, Cat. #1801) with 2% fetal bovine serum (ScienCell Cat. #0010), 1% astrocyte growth supplement (ScienCell Cat. #1852), and 1% penicillin/streptomycin solution (ScienCell Cat. #0503). These were split (using TrypLE, GIBCO) and plated at a density of 1 million cells per T75 flask every 7-9 days. All experiments were performed on early passage numbered cells (< P8).

All yeast models described in this paper were constructed in a W303α background. For validation purposes, assays were performed in different backgrounds (BY4741, W303a) and all results were consistent across the different yeast backgrounds. Unless otherwise noted, yeast were grown at 30°C in minimal synthetic culture media (Sunrise Science Products) and supplemented with 2% glucose. For all experiments involving overexpression of Yap1802p or any other genetic modifiers, the yeast were switched into 2% (w/v) galactose media upon induction. Prior to switching the carbon source to galactose, the cultures were grown in 2% raffinose for a day to metabolically adjust to the non-fermentable carbon source. All cultures were grown at 30°C under shaking conditions in an incubator. Transformations of plasmids into yeast were carried out using a standard lithium acetate protocol (Gietz and Schiestl, 2007). All genetic modifiers tested were from the yeast ORF collection (FLEXgene, Dharmacon).

Inducible expression of *APOE* isoforms in *S. cerevisiae*

In order to generate *APOE S. cerevisiae* models where protein expression could be induced in a variety of carbon sources, we employed a two-plasmid system adapted from previous work (Aranda-Díaz et al., 2017). Independence of induction reagent from carbon source was especially crucial in the study of lipid-associated processes like cellular trafficking. One component of the inducible expression system is the transcriptional regulator (ZEM) construct, a fusion of a the Zif268-DNA binding domain, the human estrogen receptor, and the Msn2 activation domain. This ZEM was expressed in a constitutive manner from an *S. paradoxus* ElFα promoter. When estradiol is added, it binds the ZEM, the complex translocates to the nucleus where it binds to a synthetic promoter (pZ), which is a modified GAL1 promoter that drives the expression of *APOE* isoforms. To capture the trafficking of APOE through the secretory pathway, the APOE isoforms were expressed with a secretory signal sequence from the protein Kar2p. The ZEM construct was singly integrated at either the TRP or YBR032W locus. The pZ-Kar2pss-APOE construct was singly integrated at either the HIS or LEU loci.

For experiments that involved comparisons with other neurodegenerative disease proteins, similar models were constructed where the 42-amino acid Aβ peptide was expressed under the control of the pZ promoter and with a Kar2p signal sequence. The TDP-43 model referenced was expressed under the same inducible promoter but did not contain a secretory pathway signal sequence.

Yeast growth curves in liquid media and spotting assays

Yeast were grown overnight to saturation, diluted in the morning and grown to logarithmic phase. Cultures were then diluted to an OD600 of 0.05 in inducing media. The OD600 was monitored on a Multiskan GO Microplate Spectrophotometer (Thermo Fischer Scientific) taking readings every 15 minutes, at a temperature of 30°C with 15 s of shaking prior to every reading. The targeted screen of endocytic modulators was conducted using the centromeric plasmid yeast ORF library (Dharmacon).

For spotting assays, yeast were grown overnight to saturation, diluted in the morning and grown to logarithmic phase. They were then normalized to a starting OD600 of 0.5, diluted in five-fold serial dilution and spotted on agar plates with inducing and selective media. Spots were photographed at 24h, 48h, and 72h after spotting.

Semi-denaturing oligomer blots

Yeast cultures were grown overnight to saturation, then diluted to an OD600 of 0.05 and grown for 8h at 30°C. Then 0.5 OD600 units of these cultures were plated on agar plates with inducing media and placed at 30°C for 15 hours. Induced yeast was then scraped from the plates and lysates were prepared using bead-beating for 10 minutes at 4°C in lysis buffer (50 mM HEPES pH 7.5, 150 mM NaCl, 2.5 mM EDTA, 1% (v/v) Triton X-100, 1 EDTA Free Mini Protease Cocktail Pellet per 5 mL of buffer, 50 mM N-ethyl-maleimide, 1 mM phenylmethylsulfonyl fluoride). Protein concentrations were measured using BCA assay and lysates were then resuspended in NativePAGE sample buffer (Thermo Fischer Scientific) and run on a 4%–12% Bis-Tris Gel in MES running buffer at 90V, at 4°C. The gel was then transferred to a PVDF membrane using the iBLOT2 dry blotting system (Thermo Fischer Scientific). Blocking and antibody incubations were performed in 5% nonfat dry milk in PBS and washes were performed with PBS with 1% (v/v)

Tween-20. Primary antibody incubations were performed overnight at 4°C. Secondary antibody incubations were performed at room temperature for 1h.

Western blots

Yeast cultures were grown to logarithmic phase and induced with estradiol for 6-12 hours. Cells were then harvested and the protein fraction was precipitated from 1.5 units of OD600 (optical density at 600 nm) culture using trichloroacetic acid. The resulting protein pellets were then resuspended in a urea-based sample buffer (2% SDS, 7M urea, 1 mM TCEP, 200 mM TRIS pH 6.8) and solubilized at 65°C for 15 minutes. Bis-Tris acrylamide gels were run at 125V and the resulting gels were transferred to nitrocellulose membranes using the iBLOT2 dry blotting system (Thermo Fischer Scientific). Membranes were blocked with 5% dry milk in PBS, and incubated overnight with primary antibodies at 4°C. For APOE blots, the polyclonal goat AB947 antibody (Millipore Sigma) at 1:500 dilution was used. PGK1 was probed using rabbit polyclonal (ABIN568371) (1:5000 dilution) and amyloid-beta was probed using the 6E10 antibody (1:1000 dilution). Quantification of blot images from the Gel Doc imaging system (BioRad) was performed using ImageJ (NIH).

Astrocyte cultures were grown to confluence in a 6-well plate. 2 wells of a confluent 6-well plate were combined and used to create a single lysate. Cells were scraped off the plate in RIPA buffer with HALT protease inhibitors and PMSF. Cold pellets were spun down at 2000xg and supernatants were boiled with sample buffer (1:6) for western blotting. Blotting was carried out using similar protocol as for yeast, however, for astrocyte blots, a Transblot (BioRAD) transfer device was used.

Reporter assays

All fluorescent reporters described (except STE3) were tagged at their endogenous loci. Due to its low endogenous expression level, STE3 was expressed constitutively from the GPD promoter using an episomal plasmid. Tagged Rab constructs were N-terminally labeled with the mNeonGreen fluorophore, whereas STE3 and MUP1 were tagged C-terminally with mKate2 and mCherry, respectively. All yeast cells were imaged or analyzed in logarithmic growth phase. Images were acquired with a Nikon Plan Apo 100x oil objective (NA 1.4). For flow cytometry analysis yeast with fluorescent reporters were grown in inducing media to logarithmic phase and then incubated with propidium iodide (10 ng/mL, Sigma Aldrich) for 5 minutes. 15,000-20,000 cells were measured using the MACSquant VYB flow cytometer (Miltenyi Biotec). Gating and analysis was performed using FlowJo v8 (FlowJo LLC).

Invertase assay

The invertase construct (pHB4, Addgene # 53462) was inserted at the endogenous SUC2 locus (selection with nourseothricin) of all strains used. *APOE*-expressing and control yeast were inoculated into fructose-containing media (SF-CSM or –URA) (Sunrise Science Products) and grown to saturation. Cultures were then inoculated into galactose media (SG-CSM or –URA) and again grown to saturation to ensure complete metabolic switch and induction of modifier expression. Cultures were then inoculated into SG media at an optical density (OD600 nm) of 0.1 in the morning and grown for 4-6h until in log phase, then diluted for overnight induction of *APOE* or control genes at OD600 nm of 0.05 in SG-URA with 0nM or 1nM β-estradiol (Sigma-Aldrich E8875) in a 96-well format. Following 24h induction, cultures were briefly centrifuged and concentrated 2 to 20-fold to roughly equilibrate OD600 before performing the invertase assay. The liquid glucose invertase assay to assess endocytic defects was performed according to previously published protocols (Dalton et al., 2015). Glucostat reagent was prepared fresh immediately prior to use (per 96 well plate: 13ml K_2HPO_4 0.1M pH7.0 (Sigma-Aldrich P3786), 26.7 μL glucose oxidase 1000U/ml (Sigma-Aldrich G7141), 33.3 μL HRP 1mg/ml (Sigma-Aldrich P6782), 66.7ul NEM 20mM (Sigma-Aldrich E1271), 200 μL *o*-dianisidine 10mg/ml (Sigma-Aldrich F5803)). Following sucrose addition, the glucostat reagent was incubated 7-9 minutes to ensure a final OD540 reading between 0.05-0.3, after which the invertase reaction was stopped with 6N HCl. Sample readings were calibrated based on freshly prepared glucose standard curves run on the same assay plate. Three independent colonies were run per yeast genotype on each plate, and each plate was run in technical duplicate.

iPSC culture, derivation, and lentiviral production

Isogenic iPSC lines were created, maintained, derived and differentiated as described previously (Lin et al., 2018). All iPS cells displayed a normal karyotype. Cells were differentiated into astrocytes according to previously published protocols (Chen et al., 2014; Lin et al., 2018). Following derivation and FACS-based purification, astrocytes were maintained in Astrocyte medium (ScienCell) and passaged every 5-7 days and re-seeded at a density of 10^{6-} cells in a T-75 tissue culture flask. All cells were used within 8 passages of the second GLAST sorting.

Lentivirus encoding PICALM-HA under the control of a *GFAP* promoter was produced according to standard protocols using lipid-mediated transient transfection of 293T cells, and standard packaging plasmids (pMD2.G, and psPAX, Addgene 12259, 12260). Following supernatant collection, the virus was concentrated using LentiX-Concentrator (Clontech, 631231) according to manufacturer's protocol. Viral titers were determined were determined using QuickTiter Lentivirus titer kit (Cell Biolabs) according to manufacturer's protocol.

Immunostaining

All staining of astrocytes for markers of endocytosis were performed in the same manner. Cells were plated in 96-well glass bottom plates (IBIDI) at a density of 10,000 cells per well. First cells were fixed in 4% paraformaldehyde for 15 minutes at room temperature

and then permeabilized using 0.2% Triton X-100 for 10 minutes at room temperature, blocked for 1 hour at room temperature using 1% normal goat serum, 1% normal donkey serum in 5% BSA in PBS. Primary antibodies were diluted according to supplier's suggestions in blocking solution and incubated overnight at 4°C. The next day, cells were washed and incubated with secondary antibodies at 1:1000 dilution for an hour at room temperature and imaged using a Zeiss LSM 710 inverted microscope. Antibodies used were as follows: EEA1 (mouse BD biosciences 610457, 1:100), Rab5 (rabbit, CST, 1:400), Rab7 (rabbit, CST, 1:100), Rab11 (rabbit, CST, 1:50). Imaging and quantification criteria are described below.

Transferrin uptake, EGF uptake, and Lysotracker staining

APOE astrocytes were seeded at a density of 10,000 cells per well of a 96-well glass-bottom plate (IBIDI). Then cells were infected with lentiviruses encoding GFAP-PICALM-HA for 5 days. The cells were then placed on ice for 5 minutes to halt endocytic processes, and either EGF conjugated to AlexaFluor555 (Thermo Fischer Scientific E35350) or transferrin conjugated to AlexaFluor647 (Thermo Fischer Scientific T23366) was added to the media at a concentration of 100 ng/mL or 25 ug/mL and the cells were incubated at 37°C for 5 minutes. Cells were then washed three times with cold PBS and fixed with 4% paraformaldehyde for 20 minutes at room temperature. The cells were then washed with PBS three times and Hoechst 33342 was added at a final concentration of 2 μM to each well and imaged using a Ziess LSM 880 Laser Scanning Confocal Microscope taking 1 um sections of 10-15 um Z stacks and analyzed using Imaris (Bitplane) and Fiji.

Lysotracker staining was performed according to manufacturer's instructions. Lysotracker Red (Invitrogen) was used at a concentration of 50 nM with an incubation at 37°C for 30 minutes. Cells were then fixed and imaged as described above.

QUANTIFICATION AND STATISTICAL ANALYSIS

Data were processed using Microsoft Excel and statistical analysis was performed using GraphPad Prism. Image data were quantified using Imaris (Bitplane) and ImageJ (NIH). For each image quantification, the parameters analyzed (puncta number per cell, puncta intensity, volume, or overall staining intensity per cell) are specified in the graph y-axis. For measurements of puncta number, size, or intensity, the Imaris "spots" tool was used. For total intensity of staining, ImageJ integrated density value was used. For "per cell" measurements, the data for the entire image were acquired and divided by the number of nuclei present in the image. Partial nuclei or cells were not counted as part of the image. All representative images are picked as the image with a quantification value closest to the mean of the distribution depicted in the graph. Details of statistical analysis for each experiment can be found in the figure legend (including test details, n, definition of significance, average, and precision metrics).